

# Electromagnetic Integration of High Power Resonant Circuits Comprising High Leakage Inductance Transformers

J. Biela, J. W. Kolar

Power Electronic Systems Laboratory, ETH Zürich  
Zürich, Switzerland

E-Mail: [biela@lem.ee.ethz.ch](mailto:biela@lem.ee.ethz.ch) / Homepage: [www.pes.ee.ethz.ch](http://www.pes.ee.ethz.ch)

**Abstract** – Known core shapes and leakage flux paths (LFP) for electromagnetically integrated transformers (EMIT) are classified and extended to new core shapes and winding structures. The distinctive feature of the classification is the orientation of the leakage flux path (magnetic shunt) with respect to the axis of the windings (perpendicular or aligned) and the direction of the compression of the core. After discussing the properties of the presented structures the low profile shapes are compared by means of volume, magnetic path length and mean turn length. The flux and current distribution of the EMIT needed for the comparison are calculated by combining fundamental frequency analysis with reluctance models. Finally, measurement results for two prototypes are presented.

## I. INTRODUCTION

Magnetic components of DC-DC converters for telecom power supplies are frequently employing planar magnetic cores in order to achieve a low profile/small height and facilitate an automated assembly. The requirements for increased power density and efficiency are met by high switching frequencies and soft switching techniques or resonant converter topologies [1].

For realising a series-parallel resonant converter the basic structure of a full bridge DC-DC converter has to be extended by a series inductance (incl. the leakage inductance of the transformer) and series capacitance as well as a parallel capacitance as shown in Fig. 1. These components can be integrated into the transformer as described in [2], with the objective of reducing the overall volume and simplifying the manufacturing. The basic principle of this electromagnetic integration is described in [3] and is shortly repeated in the following. To this end in Fig. 2(a) an isolated series-parallel resonant circuit built up with discrete components is depicted. In Fig. 2(b) the transformer has been replaced by its equivalent circuit. The series inductance of the resonant circuit is implemented by the leakage inductance of the transformer, which has to be increased or adjusted by methods discussed in section 3 of this paper.

The series capacitance is realised by the primary winding of the transformer. With this winding also a part of the leakage inductance of the transformer respectively the series inductance is implemented. The construction of the primary winding which is realised by a metal-coated dielectric wound around a ferrite core is shown in the upper part of Fig. 2(c). One end of the primary winding is connected to the copper foil P1, the second one to the foil P2. Therefore, the whole primary current  $I_1$  has to flow through the dielectric and this displacement/capacitive current  $I_{Cs}$  also contributes to the magneto motive force of the primary winding.

The secondary winding implements the parallel capacitor as well as the remaining part of the series inductance. The lower part of Fig. 2(c) reveals the construction principle. It also consists of a metal-coated dielectric, which is wound around a ferrite core. In contrast to the primary winding both ends of the secondary winding are connected to copper foil S1. Thus, the load current just flows in this foil and not through foil S2. The capacitive current  $I_{Cp}$  is driven by the secondary voltage which is induced by the varying flux excited by the primary winding. It flows from the connection between foil S1 and S2 through foil S2 where it decreases along the foil since it flows through the dielectric to foil S1 driven by the local voltage difference between the foils S1 and S2.

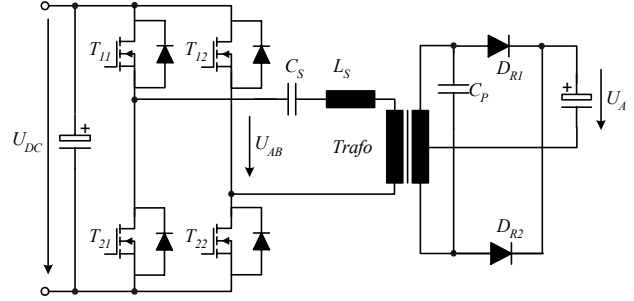


Fig. 1 Series-parallel resonant DC-DC converter

Up to now most of the implemented electromagnetically integrated transformers (EMIT) are realised by planar E-cores and windings on multilayer PCBs. The capacitance is realised by layers of material with a high permittivity [e.g. BaTiO<sub>3</sub>] in-between the copper layers. However, applying this principle of construction to high power converters leads to relatively high copper losses because of the relative large mean turn length and problems (losses/manufacturing) with the realisation of the integrated series inductance. An alternative is the use of conventional core shapes and copper foils [4], [5].

In this paper, concepts which could be applied for realising high power electromagnetically integrated high leakage inductance transformers are reviewed and new transformer constructions are proposed. In Section 2 the properties of dielectrics which are suitable for the integration of capacitors are presented briefly. Thereaf-

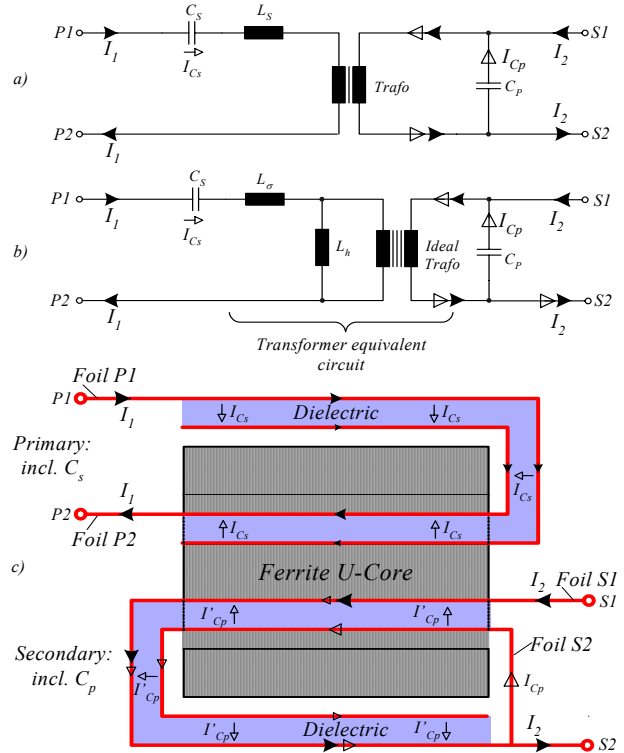


Fig. 2: (a) Series-parallel resonant circuit (b) Series inductance implemented by the leakage inductance of the transformer (c) Electromagnetic integration of the series L-C (upper) and parallel L-C (lower) branch of the circuit.

ter, in **Section 3** known core shapes and leakage flux paths are classified and extended to new geometries and winding arrangements. The distinctive feature is the orientation of the leakage flux path (magnetic shunt) with respect to the axis of the windings (perpendicular or aligned) and the profile of the core (low or cubic/conventional). In **Section 4** the presented core and winding arrangements are compared concerning the overall volume, the magnetic path length and the mean turn length based on constant power loss densities in the core and the winding. Thereafter, a model for calculating the flux and current distribution within the EMIT as required for a detailed comparison is briefly presented in **Section 5** and measurement results for two prototypes to be applied in a series-parallel resonant circuit of a 3kW converter are shown in **Section 6**. Finally, conclusions and future research aims are given in **Section 7**.

## II. DIELECTRIC MATERIALS FOR APPLICATION IN EMITS

The dielectrics suitable for the integration of a capacitor in transformer or inductor windings can be classified as follows:

- 1) Ceramic-Materials: e.g. LTCC-based HiK/Bariumtitanat [6], [7]
- 2) Plastic-Foils: e.g. Kapton / Polypropylene / Polystyrol [8]
- 3) PCB-compatible-Materials: e.g. C-Lam / RO3210 [9], [10]

The properties of some materials belonging to these groups are listed in **Table 1**. In addition to the dielectric foils the LTCC HiK-material offers excellent electrical (especially the loss factor) properties. A planar prototype has been realised (cf. fig. 10) so as to test this material.

The capacitive layers made of ceramic materials are fabricated in a sintering process, which requires specialised knowledge and equipment. Due to the brittle structure the size of the capacitive layers is limited and the thickness must be larger than a minimum value in order to ensure mechanical stability. Furthermore, different shrinking during sintering and different thermal expansion coefficients limit the sequences of layers which can be manufactured properly. Another limiting factor is the producible thickness of the metallization in a LTCC process, especially in multilayer assemblies. The thickness could be increased if the ceramic is contacted by sputtering and the thickness of the metal layer is subsequently increased by electroplating [2]. Due to the mechanical properties of the ceramic material it could be used only for planar winding structures similar to a realisation by a multi-layer PCB.

When using Kapton as dielectric the thickness of the metal foil could be increased without problems, since the foil is just connected to the Kapton with special glue [8]. This is also true for PP-/PS-foils except for foils which are contacted by metal vaporising. In this case the thickness could also be increased by electroplating. The limited temperature stability of PP-/PS-foils could be a problem if one would like to fully utilise the integrated device. This is usually no problem with Kapton foils which allow a higher maximum operation temperature. The fabrication of the winding is the same as for standard copper foils.

This is also true for PCB-compatible dielectrics, since the manufacturing is very similar to the one of standard PCBs. As with PCBs the thickness of the copper tracks usually could be up to approximately 100 microns. Larger values are also possible when

using thicker foils.

A problem of the PCB-based materials and also the foils is the low permittivity [8]. Partly, this could be compensated by low thickness which increases the achievable capacitance per area. With increasing switching frequencies the required capacitance values decrease and the necessary surface of the copper wires, which simultaneously represents the available area for the capacitor, increases due to the skin effect. Consequently, these materials are more suited for higher frequency applications.

So far, the loss factor of the materials, which is also given in table 1, has been neglected. In the rightmost column the losses in Watt at the nominal operating point for the capacitor  $C_p$  of a 3kW series-parallel resonant converter prototype are given. The losses resulting for Bariumtitanat [6], [7] or C-Lam material [9] would be far too high. The resulting value for the PP/PS-Foil is a kind of reference value for a discrete solution with KP-, MKP-, MFP- or KS-capacitors. The LTCC HiK-material, RO3210 and Kapton show higher but still reasonable losses.

Summarising the above mentioned facts:

- For planar integrated capacitors (i.e. assemblies similar to PCBs) one could use the LTCC HiK-material, which has a higher permittivity but also involves higher costs, alternatively, a kind of PCB-based material like RO3210 could be used if the required capacitance values are low. The achievable thickness of the conductor could be a limiting factor for the ceramic material.
- When using conventional (low-profile) transformers the integrated capacitor could be realised with Kapton-/PP-/PS-foils. The realisable capacitance value, however, is limited due to the low permittivity but the manufacturing costs are low.

## III. CLASSIFICATION OF CORE SHAPES AND WINDING ARRANGEMENTS

The possibilities for integrating a series inductance in a transformer by increasing its leakage inductance can be divided into two groups (**Fig. 3** and **Fig. 4**). The distinctive feature is the orientation of the magnetic shunt/leakage flux path (LFP) with respect to the axis of the winding. At the top of **Fig. 3** a transformer with cubic profile (CPT) is shown, whose LFP is perpendicular to the axis of the windings. In contrast to this, a cubic profile transformer whose LFP is aligned with the winding axis is depicted at the top of **Fig. 4**. These two main representatives can be modified in order to get low profile shapes and different winding structures as will be discussed in the following for the two groups separately.

(Note: For all the following considerations any of the two transformer windings could be used as primary or secondary winding).

### A. Perpendicular Leakage Path (PLP) and Subgroups

In **Fig. 3** the basic possibilities for realising a perpendicular leakage path (PLP) are given. In order to obtain a low profile transformer (LPT) the CPT has to be compressed in the x-, y- and z-direction [11]. The results are given in the 2<sup>nd</sup> row of **Fig. 3**.

**Z-compressed:** The most left core shape in **Fig. 3** is the well known planar core, whose windings can be realised by a PCB or (litz) wire. The disadvantage of this core shape is its relative large

Dielectric material	Permittivity	Thickness [μm]	Capacitance per 1 cm <sup>2</sup>	Breakdown Voltage [V/mm]	Loss Factor	Losses for: 110nF/100V/300kHz
LTCC HiK- Material	ca. 30..65..100	120	0.22...0.48...7.4 nF	ca. 40kV	ca. 0.001	ca. 2.07
Bariumtitanat	200..14000	ca. 200	0.89..62nF	5-20kV	ca. 0.02	ca. 41.45
PP/PS-Foils	2.2/2.4	5..10	0.19..0.38nF	ca. 200kV	0.0003	0.622
Pyralux™ (Kapton)	.4	25	0.12nF	236kV	0.003 @ 0..20GHz	6.22
C-Lam™ (Isola)	10	40	0.2nF	30kV	0.02 @ 1MHz	41.45
Rogers RO3210™	10.2	130	70pF	-	0.0027 @ 10GHz	5.60

Table 1 – Dielectric materials suitable for the integration of capacitors

winding length compared to the CPT. Additionally, it is difficult to obtain a large wire cross-section using PCB tracks as the width (x-direction) of the winding is limited (a larger window width increases the magnetic path length) and the height (z-direction if a LFP is integrated) of the layer is limited due to the skin effect. Furthermore, the windings can not be paralleled easily for increasing the cross-sectional area since standard interleaving is not possible as it could result in an unequal current sharing between the parallel windings [12]. For connecting windings in parallel with improved current sharing the repetition of the LFP as shown at the bottom in Fig. 3 is proposed. One has to interleave the windings together with the LFP. Unfortunately, in case of a parallel connection of the upper and lower winding the two leakage inductances – realised by the upper and the lower LFP – are also connected in parallel. Therefore, the leakage flux in the two LFPs is the same as with just one LFP and no parallel connected windings. This results in higher losses in the LFP or increased overall volume of the LFP in order to decrease the flux density.

The cross-sectional areas of the three legs should be adapted to the peak values of the magnetic fluxes, which occur during operation. This minimises the core losses and the overall volume and leads to equally distributed losses within the core. This holds for all core shapes.

**Y-compressed:** This shape (middle of the 2<sup>nd</sup> row in Fig.3) features a shorter winding length (comparable to the CPT) but an increased length of the magnetic path. Again, employing copper foil the cross-sectional area of the copper is limited as the width (y-direction) of the winding is limited (a larger window width increases the magnetic path length even more). Furthermore, the current distribution within the copper foils will be unequal for higher frequencies because the current is concentrating in the parts of the copper foil which are close to the LFP (reduction of magnetically stored energy in the leakage field in the air). Again, interleaving of the windings including the LFP can be done with the same disadvantages as already mentioned for the z-compressed core).

**X-compressed:** This core shape (most right one in Fig.3, 2<sup>nd</sup> row) has approximately equal mean turn and magnetic path lengths. With this core shape copper foils or (litz) wires can be used for realising the windings. Using copper foils the problem regarding the unequal current distribution within the foils, as already mentioned for the y-compressed core, exists again.

For the z-compressed core shape ceramic or PCB-compatible dielectrics and for the y- and x-compressed ones Kapton or PP/PS foils can be used for integrating a capacitor. Due to the large permittivity of the ceramic materials and the large mean turn length the largest capacitance values can be integrated into the z-compressed core shape. The lower permittivity of the dielectric foils and the shorter turn lengths result in lower capacitance values, which can be integrated, for y-compressed shape. This is especially true for the x-compressed core shape.

In the 3<sup>rd</sup> row of Fig.3 four different possibilities for realising the LFP considering the z-compressed / planar transformer as example are shown and explained in the following.

- The first possibility is to insert a block of ferrite between the primary and secondary winding. The reluctance of the leakage flux path is controlled by an air gap between the planar core and the ferrite block. However, for ensuring a low tolerance of the leakage inductance value the dimensions of the air gap have to be controlled tightly. This is a problem due to manufacturing tolerances [13]. In order to reduce the leakage field and its influence on the winding losses, the gap could be divided into several smaller gaps [14]. These smaller gaps are connected in series (ferrite block – small gap – ferrite block – small gap - ...).
- Instead of using a ferrite block in combination with an air gap one could insert a block of material which has a low permeability. The permeability of the material has to have the correct value for realising a specific value of the leakage inductance. Again, the mechanical tolerances of the core pose a problem for the industrial manufacturing. Furthermore, all known materials (FPC –

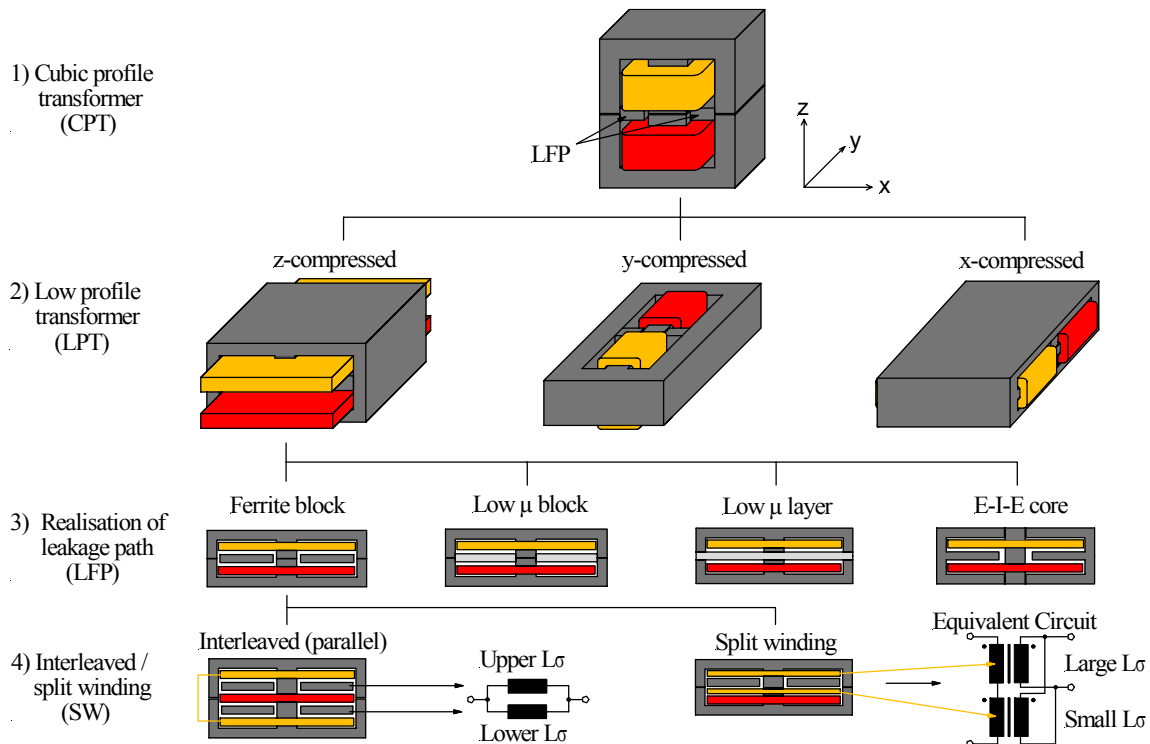


**Fig. 3 - 1<sup>st</sup> row:** Cubic profile (CPT) transformer with perpendicular leakage flux path (PLP) / **2<sup>nd</sup> row:** Compressing the CPT in x-, y- or z-directions results in low profile transformers (LPT) / **3<sup>rd</sup> row:** Four possibilities of realising the leakage flux path (LFP) considering the z-compressed transformer as example / **4<sup>th</sup> row:** *Left:* Interleaving of the windings for reducing the proximity losses (incl. equivalent circuit for the leakage inductances) / *Right:* Splitting of one winding in order to adjust the leakage inductance and to reduce the air gap length (incl. equivalent circuit for series connected splitted windings)

Epcos, 1230 - Prometheus, Vitroperm – VAC [15]–[17]) which have a low permeability cause high losses when operated at high frequencies compared to ferrite material.

- The authors of [13] proposed to place a magnetic layer consisting of a material which has a low permeability between the planar cores. This method avoids the mentioned problems concerning mechanical tolerances but reduces the magnetising inductance of the transformer, i.e. the magnetising current increases. Furthermore, the high losses of the material with low permeability pose a problem for high power applications.
- The concepts described so far are based on inserting an additional magnetic layer for the leakage flux. A new possibility would be to combine three ferrite cores, two E- and one I-core, with an air gap, which is not dependent on the mechanical tolerances of the manufacturing process. The air gap is fabricated by grinding the two E-cores, what is a standard process for fabricating air gaps with low tolerances. The disadvantages are the need for custom cores and the elaborate assembly. Therefore, the concept is economically viable only for high volume productions.

The realisation possibilities of the LFP shown for the z-compressed core also can also be applied to the y- and x-compressed cores with the same pros and cons as discussed above. Therefore, they are not discussed further for the sake of brevity.

Up to now all turns of the windings (both primary and secondary) are linked with the respective leakage flux. If the number of turns is high and the required series inductance is low a large air gap or a low permeability would be needed for adapting the size of the leakage inductance to the required value of the series inductance. The large air gap would lead to large leakage fields which could cause EMI problems and eddy current losses in the windings. In order to reduce the length of the air gap one winding could be splitted into two partial windings (SW) as depicted in the last row of Fig. 3 (the upper winding shown in light grey/orange). This reduces the number of turns linked with the leakage flux. The equivalent circuit representing this winding arrangement would be an interconnection of two transformers. One winding is connected in series and the other one in parallel. Thereby, the upper transformer represents the upper orange/light grey winding and has a large leakage inductance and the lower transformer having a small leakage inductance represents the lower orange/light grey winding. Assuming that the red/dark grey winding is shorted and considering the equivalent circuit it is obvious that only the upper part of the orange/light grey winding respectively the upper equivalent transformer mainly defines the overall leakage impedance. The reduction of the number of turns linked with the leakage flux leads to higher values for the leakage flux since the flux linkage is determined by the fixed inductance value and primary current.

The standard interleaving of the primary and secondary winding can also be applied to the parts of the windings which are not separated by the PLP. The rest of the winding must be interleaved together with the PLP as described above.

### B. Aligned Leakage Path (ALP) and Subgroups

Transformer constructions with aligned leakage path (ALP) and possibilities for realising the aligned LFP are shown in Fig. 4. In order to achieve a low profile magnetic core the cubic profile transformer (CPT) can be compressed in the x-, y- and z-direction, again. The results thereof are given in the 2<sup>nd</sup> row of Fig. 4.

**Z-compressed:** Again, this core shape is equal to the standard planar core. Usually, the windings are wound around the middle leg of the planar core and are realised by PCB tracks. In the shown structure the windings are wound around the two outer legs of the E-core and the middle leg realises the LFP. Alternatively, one winding could be arranged around the middle leg and the LFP is realised by an outer leg [18]. If the windings are realised by PCB tracks it is

important to notice, that the current distribution within the cross-section will be non-uniform for higher frequencies because the current is concentrating in the parts of the copper foil which are close to the LFP. Thus, PCB tracks lying vertically (in z-direction) on top of each other should be connected in parallel in order to increase the cross-sectional area and multiple or all turns are realised within one layer. The mean turn length is comparatively large as already described for the PLP version.

**Y-compressed:** In the middle of the 2<sup>nd</sup> row of Fig. 4 the y-compressed transformer is depicted. This core shape results in the lowest mean turn length, but also the largest magnetic path length. Despite of the skin and proximity effect the shape of the window allows for large current carrying cross-sections of the turns when using copper foil windings due to its large height (y-direction). Moreover, the large height enables the integration of relatively large capacitance values despite the short mean turn length. Since the current tends to concentrate itself within the cross-sectional area where the largest magnetic fields are (i.e. parallel to the LFP) the current is more uniformly distributed within the foil as with the PLP x- and y-compressed shape. This leads to lower copper losses.

**X-compressed:** The x-compressed version of a transformer with ALP is characterised by a large mean turn length and a medium magnetic path length. The large mean turn length and width of the window (y-direction) result in the largest area available for integrating capacitors in case copper foils are used for the realisation of the windings.

The 3<sup>rd</sup> row of Fig. 4 shows the possibilities for realising an ALP considering the z-compressed LPT as example. These are very similar to the realisation methods of the PLP except for the E-E core. Also the related problems are similar so that only the differences between the PLP and ALP are explained in the following.

- Again, the first variant is to insert a block of ferrite (or a distributed gap structure) between the primary and secondary winding.
- Alternatively, one could use standard E-cores with an air gap in the centre leg. This results in lower costs and also the problems related to manufacturing tolerances are eliminated.
- The E-E core V2 is just a variation of the winding arrangement of E-E core V1 proposed in [18]. There, the outer leg which is not enclosed by a winding generates large stray fields what could cause EMI problems.
- The shown realisation of the ALP with a low  $\mu$  block is characterised by the same problems as the corresponding realisation for the PLP.
- Besides the same problems the PLP version with a layer of low  $\mu$  material implicates the shown structure is difficult to assemble.

The shown realisation possibilities of the LFP can be applied – with the same pros and cons - to the other ALP core shapes.

In the 2<sup>nd</sup> row of Fig. 4 the low profile core shapes are shown with separate windings. Due to the separation of the windings the external leakage fields and with it the EMI problems increase what is also true for the PLP structures. This could be avoided by applying an enclosing winding (EW) structure which is shown in the 4<sup>th</sup> row of Fig. 4. With this arrangement of the windings one winding has a relatively large mean turn length because it completely encloses the LFP and also the second winding. On the one hand the large mean turn length results in high winding losses but on the other hand also offers a large area for integrating a capacitor and for cooling.

In the 5<sup>th</sup> row of Fig. 4 the top view of the EW y-compressed LP core shape is shown. As with the PLP structures it is also possible to split one winding so that not all turns are linked with the leakage flux (cf. 6<sup>th</sup> row of Fig. 4 / orange/light grey winding). Again, this reduces the required air gap length but increases the leakage flux. With the SP I split winding arrangement the outer

orange/light grey winding encloses the LFP and the red/dark grey winding. Since the fluxes in the three legs of the core approximately sum up to zero (neglecting the stray field in the window and the flux which leaks from the lateral surfaces of the core) the turns which are linked with the leakage flux and also enclose the middle leg equally could be shifted to the left leg. Consequently, the total number of turns of the orange/light grey winding is wound around the middle leg and just the turns, which are linked with the leakage flux, are wound around the left leg. This winding structure is similar to integrated magnetics [19] since it utilizes an additional winding for integrating the inductance.

Instead of using a single E-core for the EMIT it is also possible to use two separate U- or UR-cores. The one of the U-cores, whose one leg is enclosed by both windings, realises the transformer, with the other one, whose one leg is just enclosed by one winding, the inductor is realised. This assembly is similar to a separated realisation of the transformer and the inductor. The mean turn of the orange/light grey winding, however, is smaller compared to a completely discrete solution. In order to achieve a square-shaped footprint the U- / UR-cores could also be arranged side by side, as shown on the right hand side of the 7<sup>th</sup> row.

In the 8<sup>th</sup> row two U-core assemblies are shown, where the orange/light grey winding encloses both cores and the red/dark grey winding is wound separately on both cores. If the red/dark grey winding is connected in series the whole assembly behaves as the EMIT which is shown in the 7<sup>th</sup> row but with a doubled cross-sectional area of the core. In case the red/dark grey winding is connected in parallel and it is the secondary winding of a transformer the transformation ratio of the transformer could be doubled compared to the turns ratio (assuming that both U-Core assemblies are build up with the same core). Generally speaking, the transfer ratio is determined by the product of the turns ratio and the area ratio as known for matrix transformers [20]. The area ratio is equal to the cross sectional area of the core which is enclosed by the primary winding divided by the area which is enclosed by the secondary winding.

#### IV. COMPARISON OF THE COMPRESSED TRANSFORMERS

In the 2<sup>nd</sup> row of Fig. 3 and Fig. 4 six different arrangements of core, winding and LFP are presented which will be compared by means of their geometric properties (volume, mean turn/path

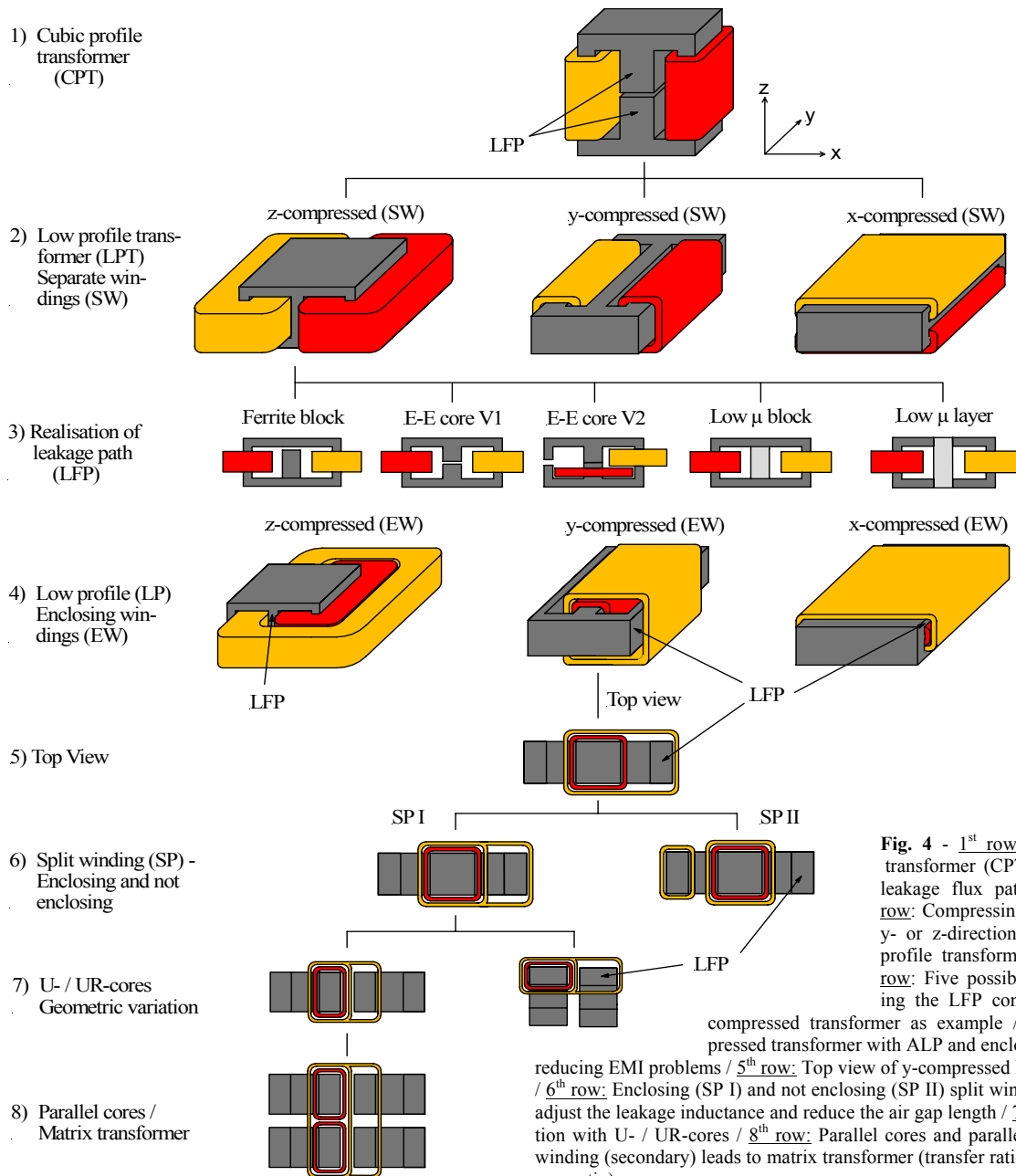


**Fig. 4** - 1<sup>st</sup> row: Cubic profile transformer (CPT) with aligned leakage flux path (ALP) / 2<sup>nd</sup> row: Compressing the CPT in x-y- or z-direction results in low profile transformers (LPT) / 3<sup>rd</sup> row: Five possibilities for realising the LFP considering the z-compressed transformer as example / 4<sup>th</sup> row: Compressed transformer with ALP and enclosing windings reducing EMI problems / 5<sup>th</sup> row: Top view of y-compressed EW transformer / 6<sup>th</sup> row: Enclosing (SP I) and not enclosing (SP II) split winding in order to adjust the leakage inductance and reduce the air gap length / 7<sup>th</sup> row: Realisation with U- / UR-cores / 8<sup>th</sup> row: Parallel cores and parallel red/dark grey winding (secondary) leads to matrix transformer (transfer ratio = turns ratio \* area ratio).

length) and the overall power loss in the following. The comparison is based on fixed cross-sectional areas for the core and the window of the core and on a constant power loss density for all assemblies i.e.  $P_{Core}/V_{Core}$ ,  $P_{\sigma}/V_{\sigma}$  and  $P_{Wdg}/V_{Wdg}$  are constant. Alternatively, one could fix the overall volume of the EMIT or the power loss density per surface area ( $W/cm^2$ ) which is related to the average rise of the surface temperature. Accordingly, the overall losses or the average temperature rise are minimized. This will be pursued in the course of future research.

In the following, the calculation of the winding losses and of the core losses is discussed. Thereafter, the derivation of the constraints for the comparison is explained, followed by the comparison of the transformer concepts.

**Winding Losses:** For calculating the power losses of the windings the skin and the proximity effects are neglected in a first step. Both effects are strongly dependent on the geometric properties of the turns and the arrangement of the winding layers and would therefore considerably complicate the calculations for a general variation of the core and winding geometries. Thus, the winding losses are equal to the DC losses. Assuming, that each winding (primary and secondary) fully utilizes half of the window area  $A_W$  the overall winding losses  $P_{Wdg}$  can be calculated as (1)

$$P_{Wdg} = 2 \cdot R I^2 = 2 \cdot \frac{N \cdot l_w}{A_{Wire} \cdot \sigma} \cdot I^2 \quad \text{with} \quad A_{Wire} = \frac{k_{Cu} A_W}{2 \cdot N} \quad (1)$$

$$P_{Wdg} = 2 \cdot \frac{2 \cdot l_w \cdot N^2 \cdot I^2}{k_{Cu} A_W \sigma} \leftarrow \frac{V_{Wdg} = A_W \cdot l_w}{k_{Cu} A_W^2 \sigma} \cdot V_{Wdg}$$

where the magnetizing current is neglected i.e.  $N_1 I_1 = N_2 I_2$  is assumed. In (1)  $A_{Wire}$  is the cross-sectional area of one turn,  $l_w$  is the mean turn length and  $V_{Wdg}$  denotes the overall volume of the winding. The number of turns is denoted by  $N$ ,  $\sigma$  is the conductivity,  $k_{Cu}$  is the winding copper fill factor and  $I$  is the effective current in the winding.

The winding current  $I$  is determined by the converter topology, the choice of component values, the operating parameters and the operating point and is approximately independent of the core and winding geometries i.e.  $I$  is constant for the comparison. Thus, with a fixed number of turns  $N$  the power loss density  $P_{Wdg}/V_{Wdg}$  is determined by the window area  $A_W$  and the winding losses  $P_{Wdg}$  are proportional to  $V_{Wdg}$ .

**Core Losses:** Assuming a uniform flux density  $B$  in the different core regions, i.e. neglecting effects like flux crowding and dimensional resonance, the flux density could be calculated as  $B = \Psi/(NA_C) = \Phi/(A_C)$  where  $\Psi$  denotes the flux linkage,  $\Phi$  is the flux in the respective leg and  $A_C$  is the corresponding cross-sectional area of the core. The same holds for the LFP. Thus, for each core region the flux density  $B$  could be calculated if the flux distribution, which will be determined in Section V, is given.

The EMIT roughly could be divided into three sections with constant flux and cross-sectional area: the LFP and two core sections. One core section carries the flux  $\Phi_1$  (linked with the primary winding) and the other one the flux  $\Phi_2$  (linked with the secondary). Assuming a symmetric core geometry  $\Phi_1$  is passing through one half of the core volume  $V_{Core,1}$  ( $=1/2 \cdot V_{Core}$ ) and  $\Phi_2$  through the second half of the volume  $V_{Core,2}$  ( $=1/2 \cdot V_{Core}$ ). Consequently, there are three different flux densities:  $B_{Core,1}$  ( $=\Phi_1/A_C$ ) in the first and  $B_{Core,2}$  ( $=\Phi_2/A_C$ ) in the second half and  $B_{LFP}$  ( $=\Phi_{\sigma}/A_{\sigma}$ ) in the LFP.

Knowing the flux densities the losses in the different sections approximately can be calculated using the Steinmetz equation since the currents and therefore the fluxes are sinusoidal. In (2) the calculation for the section of the core carrying  $\Phi_1$  is shown.

$$P_{Core,1} = C \cdot B_{Core,1}^{\alpha} f^{\beta} V_{Core,1} = C \left( \frac{\Psi_{1,Peak}}{N_1 \cdot A_C} \right)^{\alpha} f^{\beta} V_{Core,1} \quad (2)$$

$$P_{Core} = P_{Core,1} + P_{Core,2} \quad / \quad V_{Core} = V_{Core,1} + V_{Core,2}$$

The total core losses are the sum of the losses of the two sections.

As for the currents the flux distribution in the different legs also is approximately independent of the core shape and winding arrangement. This is just true in case that the stray field in the core window, which is dependent on the geometrical properties of the winding and the core, is neglected. Doing so, the power loss densities of the core  $P_{Core}/V_{Core}$  and of the LFP  $P_{\sigma}/V_{\sigma}$  are determined by  $A_C$  and the cross-sectional area of the LFP  $A_{\sigma}$ . Furthermore, the core losses  $P_{Core}$  are proportional to the core volume  $V_{Core}$ .

Consequently, by fixing the cross sectional areas  $A_C / A_{\sigma} / A_W$  and the number of turns  $N$  for the respective assembly the power loss density is also fixed. Moreover, the overall losses are proportional to the volume of the EMIT ( $V_{Core} + V_{Wdg}$ ) and by comparing the volume of the different structures for a fixed power loss density one could also compare the efficiency/losses of them.

**Minimum Loss Conditions:** By selecting a material for the core and the LFP the coefficients  $C$ ,  $\alpha$  and  $\beta$  are fixed. Additionally,  $\Psi$  and  $I$  are defined by choosing the converter topology, the component values and the operating point. Thus, all variables in the equations determining the losses (1) and (2) are fixed except for the number of turns  $N$  and the geometric properties (cross-sectional areas, volume) of the EMIT.

Assuming a fixed overall volume of the EMIT the dependency of the total losses  $P_{Core} + P_{Wdg}$  on the geometry could be expressed by a single parameter  $K$  as will be demonstrated later. Thus, there are two degrees of freedom,  $N$  and  $K$ , which can be used for minimizing the overall losses. At first, the ratio between the winding and the core losses leading to minimum overall losses is determined. This optimisation is based on the dependency of the overall losses on  $N$ . With the result the optimum number of turns is calculated. Afterwards, the ratio between the core and the winding area depending on  $K$  is optimised with respect to minimal losses. Based on this the comparison of the transformers could be performed.

In the following determination of the optimal operating point of the EMIT the LFP is neglected in order to simplify the calculations. This, however, has no influence on the results as will be explained in the following.

As shown in the preceding paragraph the optimum operating point of the EMIT is determined by the ratio of the core losses to the winding losses and the ratio of the core area to the winding area. The absolute values of the losses and the other variables do not take influence on both ratios. Considering e.g. the CPT in the 1<sup>st</sup> row of Fig. 4 the LFP just reduces the size of the window of the core. Accordingly, its influence on the geometry could be considered by changing the value of  $k_{Cu}$ . Furthermore, the flux distribution is influenced by the LFP but the absolute value of  $\Psi$  has no influence on the result in principle. The additional losses caused by the LFP could be considered by adjusting the absolute value of  $\Psi$ ,  $C$  or  $f$ . Since this difference of the absolute values of the mentioned variables has no influence on the results the LFP will be neglected.

Now the ratio of the copper  $P_{Wdg}$  losses to the core losses  $P_{Core}$  should be determined such that the overall losses are minimal independently of the core shape. Assuming that just the number of turns is variable and combining all other variables, being constant in this case, in  $G_1$  and  $G_2$  the sum of the losses could be rewritten as (3), [11].

$$P_{Wdg} + P_{Core} = \frac{4 \cdot N^2 \cdot I^2}{k_{Cu} A_W^2 \sigma} \cdot V_{Wdg} + C \left( \frac{\Psi}{N \cdot A_C} \right)^{\alpha} f^{\beta} V_{Core} \quad (3)$$

$$= G_1 \cdot N^2 + G_2 \cdot N^{-\alpha}$$

After calculating the ratio  $P_{Wdg}/P_{Core}$  using (3) and solving this expression for  $N$  the result could be used for expressing the sum of the losses independent of  $N$ .

$$\frac{P_{Wdg}}{P_{Core}} = \frac{G_1}{G_2} \cdot N^{2+\alpha} \Rightarrow N = \left( \frac{P_{Wdg} \cdot G_2}{P_{Core} \cdot G_1} \right)^{\frac{1}{2+\alpha}} \quad (4)$$

$$\xrightarrow[N \text{ in } (3, 2^{nd} \text{ row})]{\text{replacing}} P_{Wdg} + P_{Core} = f(P_{Wdg}, P_{Core}, \alpha)$$

Calculating the minimum of the overall losses by differentiating the last expression in (4) with respect to  $P_{Wdg}$  leads to a ratio (5) for the copper and the core losses which ensures minimal overall losses, which is independent of the number of turns  $N$ , the geometric properties of the core and the winding, i.e. just the influence of  $\alpha$  is remaining.

$$\frac{P_{Wdg}}{P_{Core}} = \frac{\alpha}{2} \quad (5)$$

Substituting the ratio of the losses in the expression for  $N$  in (4) with the ratio given in (5) the resulting expression for the number of turns could be used for eliminating  $N$  in the original expression (3) for the overall losses. Consequently, the overall losses depend only on the geometric properties of the EMIT (6).

$$\frac{P_{Wdg} = \frac{\alpha}{2} \text{ in } (4)}{P_{Core}} \rightarrow N = \left( \frac{\alpha \cdot G_2}{2 \cdot G_1} \right)^{\frac{1}{2+\alpha}} \quad (6)$$

$$\xrightarrow[N \text{ in } (3, 1^{st} \text{ row})]{\text{replacing}} P_{Wdg} + P_{Core} = f(A_C, A_W, V_{Core}, V_{Wdg})$$

Since the overall volume is fixed the last degree of freedom is the ratio of the window area to the cross-sectional area of the core  $A_W = K \cdot A_C$  as will be shown in the following. Assuming quadratic cross-sectional areas of the core and the window and U-shaped cores and windings which enclose each other the geometric properties of the EMIT can be expressed as (7).

$$V_{Core} = A_c l_c = A_c (4\sqrt{A_c} + 4\sqrt{KA_c}) \quad (7)$$

$$V_{Wdg} = A_w l_w = K \cdot A_c (4\sqrt{KA_c} + 4\sqrt{A_c})$$

Thus, the proportional factor  $K$  also defines the ratio of the volume of the winding to the core volume. With the constraint of the fixed overall volume  $V_{EMIT}$  of the EMIT the cross-sectional area of the core  $A_c$  could be expressed as (8).

$$A_c = Z^{\frac{2}{3}} \text{ with } Z = \frac{V_{EMIT}}{4(1 + \sqrt{K} + K + \sqrt[3]{K})} \quad (8)$$

After eliminating the number of turns  $N$  in (3) as described above and using (7) and (8) to replace  $A_c$ ,  $A_w$ ,  $V_{Wdg}$  and  $V_{Core}$  by a function of  $K$  the overall losses just depend on the ratio  $K$  of the cross-sectional area of the window and the core. Now, this expression could be differentiated with respect to  $K$  and the optimum ratio  $K$  for minimal overall losses could be calculated. The resulting expression for the optimum  $K$  is only a function of  $\alpha$ . As it is very long and complex correlation it will not be presented for the sake of

brevity.

Assuming  $\alpha = 2$ , what is approximately valid for high frequency ferrites, the optimum value of  $K$  is one i.e. that  $A_C = A_W$  and  $V_{Wdg} = V_{Core}$  (cf. (7)). Since for  $\alpha = 2$  also the ratio of the copper losses to the winding losses is equal to one, the average power loss densities of the core and the winding are also equal.

As can be seen in (9) the loss coefficient  $\alpha$  takes strong influence on  $K$ .

$$\alpha = 2.2 \rightarrow K \approx 0.88$$

$$\alpha = 1.8 \rightarrow K \approx 1.2 \quad (9)$$

**Comparison of transformer concepts:** Recapitulating the preceding calculations, the cross-sectional areas  $A_C$  and  $A_W$  and the number of turns are fixed for a minimum power loss design as soon as the material of the core, the overall volume of the EMIT and the operating point are defined.

In the following the six different transformer designs will be compared for  $\alpha = 2$  i.e. the cross-sectional areas  $A_C$  and  $A_W$  are equal. For the transformer comparison the cross-sectional areas of the window and the core no longer will be quadratic as has been assumed for the derivation of the minimal loss conditions. Accounting for the non quadratic areas results in complicating the calculations for a general variation of the core and the window considerably. Since the overall losses do not depend very much on the value of  $K$  the ratio of core area to window area is set to one,  $K=1$ , even for non quadratic core shapes.

Since the nominal output power of the considered series-parallel converter is 3kW (cf. Table 3) an ELP 64 core is chosen as reference. This core is suitable for power transformers in the range of several kW and shows an area product of  $A_C \cdot A_W = 519\text{mm}^2 \cdot 221\text{mm}^2 \approx 115.000\text{mm}^4$ . With the given area product the cross-sectional areas of the EMIT can be calculated by:  $A_C = A_W = A_\sigma / 1.2 = 339\text{mm}^2 \approx \sqrt{115.000\text{mm}^4}$ .

The cross-sectional area of the LFP  $A_\sigma$  is chosen according to the ratio between the flux  $\Phi_l$  through the primary winding and the leakage flux  $\Phi_\sigma$  so that the flux density in the LFP is equal to the maximum flux density in the core.

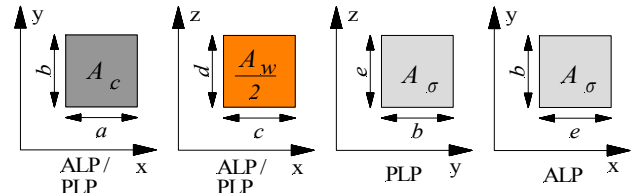


Fig. 5 Definition of the five variables describing the geometric properties of the core, winding and leakage flux path (ALP / PLP) arrangement

The overall volume of a comparable assembly with an ELP 64 core including the LFP and the winding is  $116000\text{mm}^3$  and the height is 28.4mm. Despite the fact that the curves in Fig. 6 are plotted for

special values of the cross-sectional areas the characteristics and the relative positions of the curves are representative for a wider range of cross-sectional areas. Moreover, the ratio between the cross-sectional area of the core  $A_C$  and the cross-sectional area of the LFP  $A_\sigma$  has only a small influence on the basic shape of the curves.

	ALP			PLP		
x-Dim.: $l_x$	$2 \cdot a + 4 \cdot c + e$			$2 \cdot a + 2 \cdot c$		
y-Dim.: $l_y$	$b + 2 \cdot c$			$b + 2 \cdot c$		
z-Dim.: $l_z$	$2 \cdot a + d$			$a + 2 \cdot d + e$		
$V_{Core}$	$2 \cdot a \cdot b \cdot (2 \cdot a + 2 \cdot c + d + e) + b \cdot d \cdot e$			$2 \cdot a \cdot b \cdot (a + c + 2 \cdot d + e) + 2 \cdot e \cdot b \cdot c$		
$V_{Wdg}$	$4 \cdot c \cdot d \cdot (a + b + 2 \cdot c)$			$4 \cdot c \cdot d \cdot (a + b + 2 \cdot c)$		
$l_w$	$2 \cdot (a + b) + 4 \cdot c$			$2 \cdot (a + b) + 4 \cdot c$		
$l_c$	$2 \cdot (2 \cdot a + 2 \cdot c + d + e)$			$2 \cdot (a + c + 2 \cdot d + e)$		
Cross-sectional areas	Core:	$A_C = a \cdot b$		Core:	$A_C = a \cdot b$	
	Winding:	$A_W = 2 \cdot d \cdot c$		Winding:	$A_W = 2 \cdot d \cdot c$	
	LFP:	$A_\sigma = 2 \cdot b \cdot e$		LFP:	$A_\sigma = 2 \cdot b \cdot e$	
Height	z-compressed	y-compressed	x-compressed	z-compressed	y-compressed	x-compressed
	$H = l_z = 2a + d$	$H = l_y = b + 2c$	$H = l_x = 2a + 4c + e$	$H = l_z = a + 2d + e$	$H = l_y = b + 2c$	$H = l_x = 2a + 2c$

Table 2 – Definition of the core and winding parameters and equations for the comparison

By fixing the cross-sectional areas and the window area three variables are determined. The geometric dimensions of the EMIT, however, are described by five independent variables. One possible set of variables is defined in Fig. 5. The relationships between these variables and the cross-sectional areas, window area, volume and lengths are given in the upper rows of Table 2.

Since the EMITs should have a low profile the fourth variable is fixed by determining the maximum height of the device. The fifth variable is used to minimise the volume/losses respectively the footprint area with the constraint that the variables  $a$ ,  $b$ ,  $c$ , and  $d$  are larger than a certain minimum value (3mm in the considered comparison). In the last four rows of Table 2 the four above explained constraints for the comparison of the different core shapes are given.

The volumes, the mean path lengths and the mean turn lengths for the six arrangements are shown in Fig. 6. As a kind of a reference the values for the assembly using an ELP 64 core are included (Attention: The height of the ELP 64 core assembly is not varying).

The z-compressed core shape with a PLP shows the lowest volume and the shortest mean path length for a wide range of heights but also the largest mean turn length. The large mean turn length and the LFP arrangement which in principal tends to a strongly non-uniform current density could lead to large copper losses. The effects leading to a non-uniform current density have been neglected in the preceding comparison but are part of the future research.

The x- and y-compressed core shapes with an ALP principally tend to a more uniform current density but showing a larger volume.

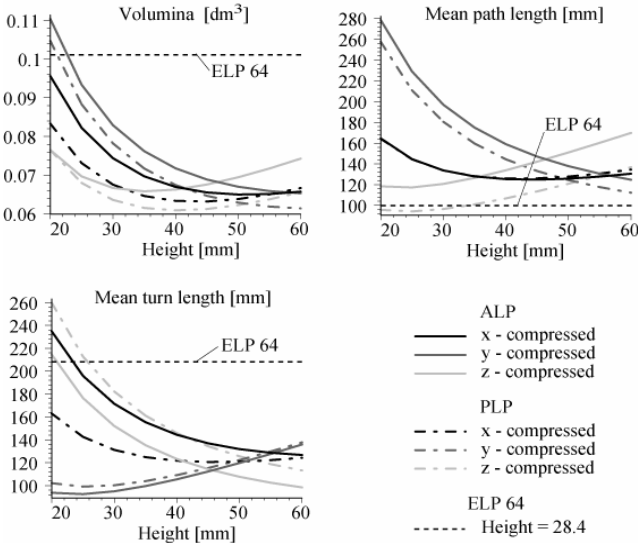


Fig. 6 Comparison of the volumes, the mean path lengths and the mean turn lengths of the six compressed core shapes. Reference: ELP 64 core.

## V. DESIGN OF EMITs USING MAGNETIC RELUCTANCE MODEL COMBINED WITH FUNDAMENTAL FREQUENCY ANALYSIS

For calculating the losses of the EMIT and determining the power loss densities one has to calculate the currents in the windings and the flux distribution in the core and LFP. At first, however, the values of the resonant circuit components must be determined. This could be done e.g. based on a procedure described in [21]. The results for the considered prototype are given in Table 3. For given component values the currents and the fluxes can be calculated by an AC equivalent model as explained in the following.

Since the resonant network attenuates the higher harmonics of the voltages and currents in the series-parallel resonant converter (cf. Fig. 1) both quantities can be calculated by classical AC analysis [22], [23]. Applying the proposed method in [23] results in the

equivalent AC network for the converter of Fig. 7 (left hand and right hand part of the circuit).

This model has been extended by a reluctance model of the EMIT which allows the calculation of the magnetic fluxes and/or magnetic flux densities in the different sections of the core. Also the phase shift between the different fluxes, i.e. leakage and main flux, is considered. Since the leakage flux adds or subtracts geometrically to/from the main flux in the different core sections the consideration of the phase shift is necessary in order to get exact results.

In Fig. 8, where the real axis of the coordinate systems is aligned to the phasor of the primary current, the flux phasors are shown for operation of the EMIT at nominal output power. The corresponding absolute values are given in Table 3. Since the phase

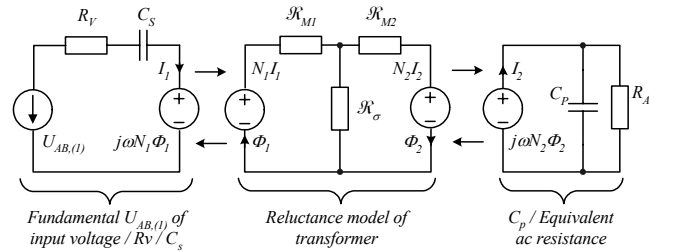


Fig. 7 Fundamental frequency equivalent model of the series-parallel resonant converter including a magnetic reluctance transformer model for calculating the flux densities in the sections of the transformer. The shift between the primary current and the leakage flux is relatively small the magnitude of the leakage flux could be approximated as  $|\Psi_{\sigma,peak}| \approx L_S \cdot I_{1,peak}$ . Due to the large phase shift between the fluxes the assumption that the absolute values add up to zero would lead to comparatively large errors.

With the presented model it is also possible to calculate the voltages and currents of the windings as well as the amplitude of the fundamental of the input voltage  $U_{AB,(1)}$  and the duty cycle of the converter for a given output voltage and load current.

The resulting flux densities can be used to calculate the core losses by means of the Steinmetz equation [24]. With the primary and secondary current the losses in the windings could be calculated by means of analytical (1-D approximation) calculations [2], [25]. The analytical approach could be used for optimizing the thickness of the copper foil respectively of the PCB track for the given operation frequency and current in order to achieve minimum copper losses. In case the resulting losses are still too high a further reduction could be achieved by interleaving (4<sup>th</sup> row of Fig. 4) or increasing the foil or track width (i.e. changing the geometry of the core).

By combining the proposed reluctance model and the 1-D analytical model of the copper losses the overall losses and/or the power loss density could be optimised by varying the geometric properties. There, the copper and the core losses have to be considered simultaneously as both loss components interdepend by means of the core and winding geometry as will be shown in a future publication of the authors.

## VI. EXPERIMENTAL ANALYSIS OF A CONVENTIONAL EMIT WITH ALP AND A PLANAR EMIT WITH PLP

In Fig. 9 a prototype of the cubic profile transformer with ALP and enclosing secondary foil winding is shown. The realisation is with a standard E65 core and Kapton foils as dielectric. The corresponding measurement results for an output power of 1 kW / 48 V are given

Output power	3kW
Switching frequency	300..600kHz
Series capacitance	35nF
Parallel capacitance	110nF
Series inductance	12.5μH
Series Current $I_{1,peak}$	28.2A
$ \Psi_{1,Peak}  = N \cdot  \Phi_{1,Peak} $	295 μVs
$ \Psi_{2,Peak}  = N \cdot  \Phi_{2,Peak} $	155 μVs
$ \Psi_{\sigma,Peak}  = N \cdot  \Phi_{\sigma,Peak} $	350 μVs

Table 3 – EMIT Specification



Fig. 9 Prototype of the conventional CP transformer with ALP



Fig. 10 Prototype of LP z-compressed transformer with PLP

in Fig. 11. These results verify the enclosing windings concept. Furthermore, a close correspondence of the theoretical considerations and measurement results is given. Fig. 10 shows a realisation of the z-compressed transformer with PLP which applies the new LTCC-HiK material for the integration of the capacitors. This assembly proves the good electrical characteristics of the dielectric and therefore will be further investigated in a next step.

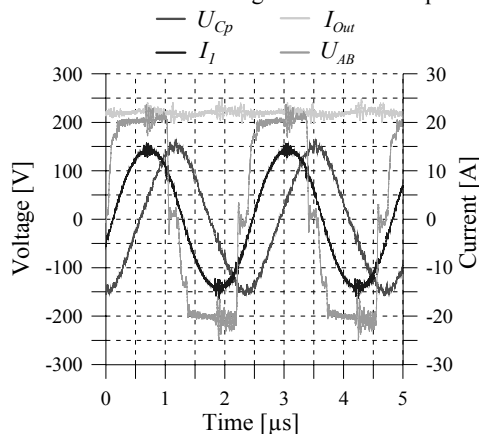


Fig. 11 Measurement results for the conventional CP transformer (Fig. 9)

## VII. CONCLUSIONS

The integration of capacitors into a transformer imposes only small restrictions on the transformer design. Planar winding designs can be realised as conductor tracks on ceramic or special PCB-material. Conventional windings can only be realised by copper and dielectric foils which only have a low permittivity i.e. the value of the capacitance, which could be integrated, is limited.

In contrast to this the integration of an inductance into a transformer influences the design to a greater extent. Due to the skin and proximity effect the current concentrates in a thin layer of the conductor which is approximately lying in parallel to the LFP. Thus, with a PLP the z-compressed core, which is most suitable for windings realised with PCBs, shows the largest current carrying layer and an approximately uniform current distribution within the cross-sectional area. For the y- and x-compressed EMIT the current is concentrating close to the LFP and therefore the current density is strongly non-uniform.

For the above mentioned reasons the largest current carrying layer and an approximately uniform current distribution is given for the y- and x-compressed core shapes with ALP.

Comparing the different designs the z-compressed core with PLP shows the lowest volume for a wide range of heights. However, it is also characterised by the largest mean turn length and therefore the highest DC winding losses. Furthermore, the realisation of the LFP is complicated by manufacturing tolerances.

In the course of future research the comparison of the different transformer designs will be extended to the constraints of fixed power losses per surface area, fixed temperature rise and fixed volume. Moreover, the loss model of the transformer will be extended to high frequency effects like skin or proximity effect. This model will also be used for optimising the core shape for different operation conditions.

## References

- [1] G. A. Ward, and A. J. Forsyth, "Topology selection and design trade-offs for multi-kW telecom DC power supplies," in *Conf. Publ. No. 487 International Conference on Power Electronics, Machines and Drives*, June 2002, pp. 439 -444.
- [2] J. T. Strydom, "Electromagnetic Design of Integrated Resonator-Transformers," Ph.D. Thesis, Rand Afrikaans University, South Africa, 2001.
- [3] M. C. Smit, J. A. Ferreira, and J. D. van Wyk, "Application of transmission line principles to high frequency power converters," in *Proc. 23<sup>rd</sup> Annu. Power Electronics Specialists Conference*, vol. 2, June 1992, pp. 1423 -1430.
- [4] R. Reeves, "Choke-capacitor hybrid as a fluorescent lamp ballast," *Proc. Inst. Elect. Eng.*, vol. 12, no. 10, October 1975, pp. 1151-1152.
- [5] J. C. Crebier, T. Chevalier, K. Laouamri, and J. P. Ferrieux, "Study and analysis of wounded integrated L-C passive components," in *Proc. 32<sup>nd</sup> Annu. Power Electronics Specialists Conference*, vol.4, June 2001, pp. 2137 -2142.
- [6] W. A. Cronje, J.D. van Wyk, and M.F.K. Holm, "High-Permittivity Ceramic Dielectrics for Tuning Transmission in Power Electronic Converters," in *Proc.42<sup>nd</sup> Annu. Electronic Components and Technology Conference*, May 1992, pp. 601 -606.
- [7] W. Chen, X. Wang, B. Liu, W. Shang, Q. Liu, and S. Chen, "Dielectric loss of BaTiO<sub>3</sub>-based high voltage ceramic capacitor under high field strength," in *Proc. Int. Symposium on Electrical Insulating Materials*, Sept. 1998, pp.121 -122.
- [8] *Pyralux Flexible Composites*, DuPont Electronic Materials, [www.dupont.com](http://www.dupont.com), 2003.
- [9] J.A. Ferreira, E. Waffenschmidt, J.T. Strydom, and J.D. van Wyk, "Embedded capacitance in the PCB of switch mode converters," in *Proc. 32<sup>nd</sup> Annu. Power Electronics Specialists Conference*, vol. 1, June 2002, pp. 119 -123.
- [10] E. Waffenschmidt, J.A. Ferreira, "Embedded passives integrated circuits for power converters," in *Proc. 33<sup>rd</sup> Annu. Power Electronics Specialists Conference*, vol. 1, June 2002.
- [11] B. Carsten, "Magnetic Design Workshop – What the Textbooks Don't Tell You," in *Proc. of Power Conversion Electronics*, Sept. 1995, pp. 177 – 248.
- [12] R: Prieto, J: A: Cobos, O. Garcia, P. Alou, and J. Uceda, "Using parallel windings in planar magnetic components," in *Proc. 32<sup>nd</sup> Annu. Power Electronics Specialists Conference*, vol. 4, June 2001, pp. 2055 -2060.
- [13] M. Meinhardt, M. Duffy, T. O'Donnell, S. O'Reilly, J. Flannery, and C. O Mathuna, "New method for integration of resonant inductor and transformer-design, realisation, measurements," in *Proc. 14<sup>th</sup> Annu. Applied Power Electronics Conference and Exposition*, vol. 2, March 1999, pp. 1168 -1174.
- [14] C. R. Sullivan, and H. Jiankun, "AC resistance of planar power inductors and the quasidistributed gap technique," *IEEE Trans. Power Electronics*, vol.: 16, Issue: 4, July 2001, pp. 558 – 567.
- [15] *Ferrite Polymer Composites (FPC)*, Epcos Ferrite Materials, [www.epcos.com](http://www.epcos.com), 2004.
- [16] *Pulververbundwerkstoff 1230*, Sintermetalle Prometheus, [www.smp-online.com](http://www.smp-online.com), 2004.
- [17] *und nanokristalline Werkstoffe – Vitroperm*, Vacuumschmelze, <http://www.vacuumschmelze.de>, 2004.
- [18] P. Goubrier, Y. Lembeye, and J.P. Ferrieux, "Design and Characterisation of an integrated planar L-C-T Component", in *Proc. Annu. EPE*, 2003, Toulouse.
- [19] B. Yang, R. C. Chen, and F. C. Lee, "Integrated magnetic for LLC resonant converter," in *Proc. 17<sup>th</sup> Annu. Applied Power Electronics Conference and Exposition*, vol. 1, March 2002, pp. 346 – 351.
- [20] K. K. Sum, "Design and Application of matrix transformers," in *Proc. Annu. High frequency power conversion*, May 1990, pp. 160 -173.
- [21] F. Cavalcante, and J. W. Kolar, "Design of a 5kW high output voltage series-parallel resonant DC-DC converter," in *Proc. 34<sup>th</sup> Annu. Power Electronics Specialist*, vol. 4, June 2003, pp. 1807 -1814.
- [22] R. L. Steigerwald, "A comparison of half-bridge resonant converter topologies," *IEEE Trans. Power Electronics*, vol. 3, Issue: 2, April 1988, pp. 174 -182.
- [23] A. J. Forsyth, G. A. Ward, and S. V. Mollov "Extended fundamental frequency analysis of the LCC resonant converter," *IEEE Trans. Power Electronics*, vol. 18, Issue 6, Nov. 2003, pp. 1286 – 1292.
- [24] C. P. Steinmetz, "On the law of hysteresis," in *Proc. IEEE*, vol. 72, Feb. 1984, pp. 196-221.
- [25] J. A. Ferreira, "Electromagnetic modelling of power electronic converters," *Kluwer Academic Publishing – Dordrecht (Netherlands) / Norwell (Massachusetts, USA)*, 1988